ACS APPLIED MATERIALS & INTERFACES

www.acsami.org

Research Article

Construction of N-Rich Aminal-Linked Porous Organic Polymers for Outstanding Precombustion CO_2 Capture and H_2 Purification: A Combined Experimental and Theoretical Study

Debabrata Chakraborty,[⊥] Rupak Chatterjee,[⊥] Saptarsi Mondal, Sabuj Kanti Das, Vipin Amoli, Minhaeng Cho, and Asim Bhaumik*

Cite This: *ACS Appl. Mater. Interfaces* 2023, 15, 48326−48335

Read Online

ACCESS | Metrics & More | Article Recommendations | Supporting Information

ABSTRACT: A large number of scientific investigations are needed for developing a sustainable solid sorbent material for precombustion CO_2 capture in the integrated gasification combined cycle (IGCC) that is accountable for the industrial coproduction of hydrogen and electricity. Keeping in mind the industrially relevant conditions (high pressure, high temperature, and humidity) as well as good CO_2/H_2 selectivity, we explored a series of sorbent materials. An all-rounder player in this game is the porous organic polymers (POPs) that are thermally and chemically stable, easily scalable, and precisely tunable. In the present investigation, we successfully synthesized two nitrogen-rich POPs by extended Schiff-base condensation reactions. Among these two porous polymers, **TBAL-POP-2** exhibits high CO_2 uptake capacity at 30 bar pressure (57.2, 18.7, and 15.9 mmol g^{-1} at 273, 298, and 313 K temperatures, respectively). CO_2/H_2 selectivities of **TBAL-POP-1** and **2** at 25 °C are 434.35 and 477.93, respectively. On the other hand, at 313 K the CO_2/H_2 selectivities of **TBAL-POP-1** and **2** are 296.92 and 421.58, respectively. Another important feature to win the race in the search of good sorbents is CO_2 capture capacity at room temperature, which is very high for **TBAL-POP-2** (15.61 mmol g^{-1} at 298 K for 30 to 1 bar pressure swing). High BET surface area and good mesopore volume along with a large nitrogen content in the framework make **TBAL-POP-2** an excellent sorbent material for precombustion CO_2 capture and H_2 purification.

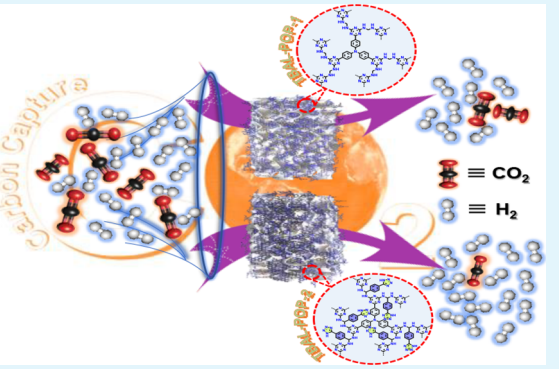

KEYWORDS: *porous organic polymers, precombustion CO_2 capture, H_2 purification, CO_2/H_2 selectivity, high-pressure CO_2 uptake*

INTRODUCTION

Any additional increase in the CO_2 concentration by the anthropogenic sources into the atmosphere should be mitigated from its current level to minimize the climate change that can badly affect the world in the future. On the other hand, to meet the high energy demand for urbanizing the world, carbon-based fossil-fuel consumption increases the CO_2 concentration in the atmosphere. In February 2023, the CO_2 concentration in the atmosphere was 420.41 ppm.[1] The Intergovernmental Panel on Climate Change (IPCC) estimates that in the absence of a mitigation process, the global carbon dioxide concentration would climb from 600 to 1550 ppm in 2100.[2] 2021 IPCC report also states that the global temperature will increase 1.5% by 2030 to 2052.[3] Among various potential solutions, CO_2 capture and sequestration (CSS) is one of the most promising approaches to mitigate the CO_2 from the atmosphere. CSS technology has been developed for application in coal and fuel-based power generation industries at various stages like precombustion, postcombustion, and oxy-fuel combustion. Among these, one of the promising processes is precombustion CO_2 capture that separates CO_2 from the mixture of CO_2 and H_2, which is formed by the gasification of coal in the integrated gasification combined cycle (IGCC). In the IGCC process, the product gas mixture composed of 40% CO_2 and 60% H_2 leaves from the water−gas shift column at high pressure (>20 bar).[4−6] To get the high-purity H_2 as a clean fuel, separation is required from the former mentioned CO_2/H_2 gas mixture. Among the various approaches for separating the gas mixture, adsorptive separation is one of the easiest and cost-effective methods, where particularly one gas component more strongly interacts with the internal surface of the porous materials.[7] In the adsorptive gas separation process, the mixture of gas is exposed to the bed filled with the porous sorbent material, and one gas component is mainly adsorbed by

Received: August 8, 2023
Accepted: September 19, 2023
Published: October 3, 2023

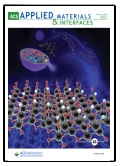

pressure swing adsorption (PSA), temperature swing adsorption and vacuum swing adsorption.[8−11] The economic viability and simplicity is the main driving force for the use of PSA as a gas separation process that separates particular gas species from the gas mixture according to their adsorption affinity or kinetics of the species with respect to sorbent materials. The significant features in designing a good sorbent material for CO_2 is high selectivity, high uptake capacity, and high working capacity. Also, it is important that the sorbent material should have good thermal and chemical stabilities because this industrial gas separation process passes through very harsh conditions (high temperature and gas mixture contains acid gases, water vapors, etc.).[12] Typically used solid sorbents like zeolites and porous carbons did not fulfill all requirements due to their low working capacities and/or low CO_2/H_2 selectivity.[13−15] Various porous materials with a good CO_2 adsorption capacity at low pressure as well as high pressure, such as metal organic frameworks,[16−18] porous organic polymers,[19−27] and covalent organic frameworks,[28−31] have been used. However, to the best of our knowledge, most of these porous materials were studied for postcombustion CO_2, and only few studies were reported on precombustion CO_2 capture, i.e., high-pressure CO_2 uptake.[32,33] The stored CO_2 can be reduced to value-added chemicals like methanol, formic acid, and so forth through high-pressure hydrogenation.[34]

Herein, we report the synthesis of two nitrogen-rich porous organic polymers **TBAL-POP-1** and **TBAL-POP-2** (TBAL = triazine-based amine linked) by extended Schiff-base condensation reaction under solvothermal condition. Due to their high specific surface area, abundance of nitrogen in the framework, and excellent thermal and chemical stabilities, both porous polymers are evaluated as a potential candidate for precombustion CO_2 capture and H_2 purification. The high-pressure CO_2/H_2 separation of both polymers is thoroughly investigated using equilibrium pure gas uptake and the initial selectivity method. The working capacity of both polymers is also calculated from pure CO_2 sorption isotherm. Our experimental investigations suggested that the increasing mesoporosity, surface area, and nitrogen-rich surface in the framework help good CO_2/H_2 separation.

RESULTS AND DISCUSSION

The **TBAL-POP-1** and **2** materials were synthesized through the simple Schiff base condensation reaction of 6-(4-(bis(4-(4,6-diamino-1,3,5-triazin-2-yl)phenyl)amino)phenyl)-1,3,5-triazine-2,4 diamine (TPDATPA) with formaldehyde and 4-(1H-tetrazol-5-yl)benzaldehyde, respectively (Figure 1a). The resultant yellow solid products are insoluble in common organic solvents due to the high degree of cross-linking in the porous polymer. The synthetic procedure (Supplementary Note 2) and ^{1}H NMR (Supplementary Note 3, Figures S1A,B and S2A) and ^{13}C NMR (Supplementary Note 3, Figures S1C and S2B) data of monomer units are described in ESI.

Spectroscopic Analysis. In order to confirm the successful synthesis of the polymeric network, all polymers were characterized by Fourier transform infrared (FT-IR) and ^{13}C cross-polarization magic angle spinning (CP/MAS) NMR spectroscopy. The FT-IR spectra in Figure 2a show that the hexamine (primary amine)-containing monomer TPDATPA has two broadbands around 3480−3300 cm^{-1} (−NH stretching) and 3250−3050 cm^{-1} (−NH_2 stretching) which confirm the presence of the primary amine group in the monomer unit. The IR spectra of the two polymers, **TBAL-POP-1** and **2**, display that there is only one broadband present

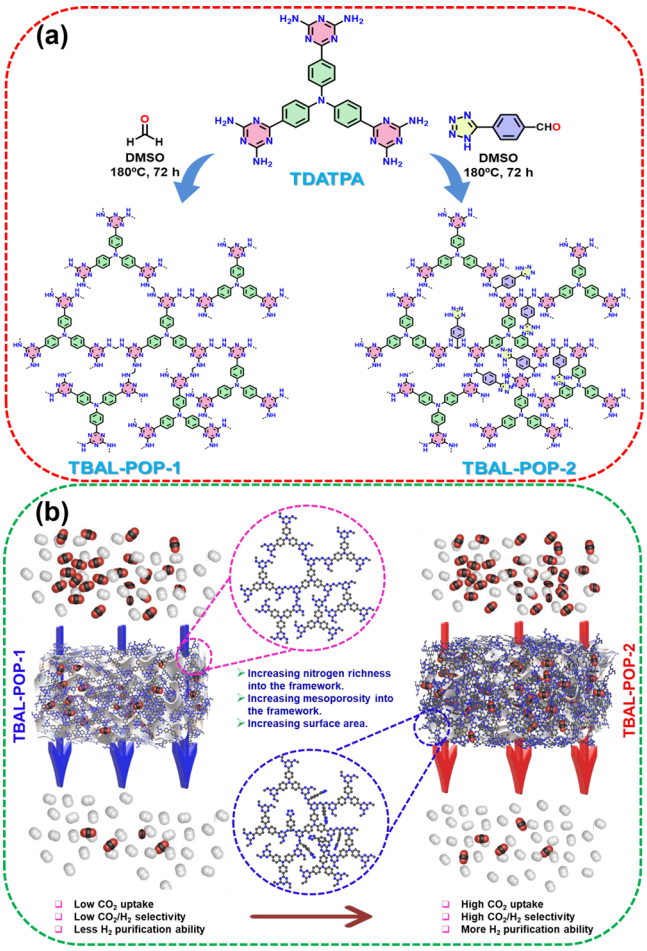

Figure 1. (a) Schematic representation of the synthesis of **TBAL-POP-1** and **TBAL-POP-2.** (b) Modular representation of CO_2/H_2 separation by **TBAL-POP-1** and **TBAL-POP-2** and an overall conceptual visualization.

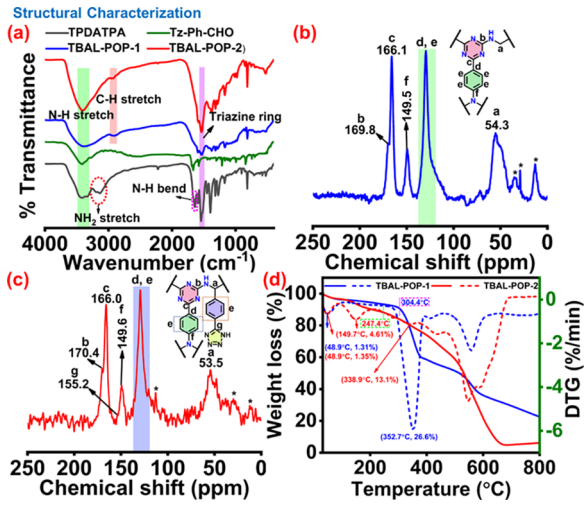

Figure 2. Characterization of **TBAL-POP-1** and **TBAL-POP-2**: (a) FT-IR spectra of all monomers and the two porous polymers **TBAL-POP-1** and **TBAL-POP-2.** (b,c) Solid-state ^{13}C−CP MAS NMR spectra of **TBAL-POP-1** and **TBAL-POP-2.** (d) TGA profile of the polymers.

https://doi.org/10.1021/acsami.3c11732
ACS Appl. Mater. Interfaces 2023, 15, 48326−48335

around 3415 cm^{-1}, and the another one (3250−3050 cm^{-1}) is missing which was present in the TPDATPA monomer unit, and this suggests the formation of aminal linkage (−C−NH−) in the polymers.[35] We also extend our clarification on the condensation reaction by observing the absence of C═O (1690 cm^{-1}) stretching of aldehyde and $-NH_2$ deformation band (1650 and 1660 cm^{-1}) of the TDATPA monomer in both the polymers.[23,36] A strong peak at 1540 cm^{-1} (characteristic peak of triazine ring) is present in TPDATPA monomer and two polymers.[23] The absence of the imine (−C═N) stretching band at 1620 cm^{-1} and the presence of a very wide band at roughly 3415 cm^{-1} imply the creation of two distinct polymer networks via −C−NH− bonding.

The solid-state ^{13}C CP/MAS NMR spectra also confirm the construction of two polymeric networks, represented in Figure 2b,c. In these two spectra, we found peaks in the same regions, e.g., 53−54, 129−130, 145−150, and 166−170 ppm, which represents methylene, unsubstituted benzene, substituted benzene, and triazine ring containing carbon, respectively.[23,31] Two types of C−N linkages, such as imine (−C═N) and secondary amine (−C−NH−), can be produced by the Schiff base condensation reaction. A secondary amine linkage (−C−NH−) may explain the disordered packing of **TBAL-POP-1** and **2** nanoparticles at about 54 ppm, which is caused by secondary amine linkage.[23] The primary difference between these two polymeric structures is that **TBAL-POP-2** contains a tetrazole moiety, and the peak of this tetrazole carbon is present around 153−155 ppm[37] in Figure 2c. For more clarity, we have also provided the solid-state ^{13}C NMR spectra of those polymers compared with the liquid ^{13}C NMR of the corresponding monomer units in Figure S3A,B in ESI (Supplementary Note 4). This analysis confirms the formation of the aminal-linked polymeric network.

Powder XRD, Elemental Analysis, Thermal Stability, and Chemical Stability. The wide-angle powder X-ray diffraction (XRD) pattern of the two polymers are shown in Supplementary Note 5, Figure S4, ESI. Both polymers **TBAL-POP-1** and **TBAL-POP-2** showed a broad peak in the range of 2θ value 17−35°, which could be attributed to the formation of the amorphous polymeric network. The construction of a crystalline covalent organic framework was geometrically unfavorable via aminal linkage between the hexamine monomer and the two aldehydes. Thus, we get amorphous polymeric materials with broad wide-angle peaks. The elemental analysis of the two polymers was investigated by using CHN analysis. CHN analysis shows that **TBAL-POP-1** contains C = 50.13%, H = 3.97%, and N = 24.15%; on the other hand, **TBAL-POP-2** contains C = 52.88%, H = 3.22%, and N = 29.22%. From the result, we can clearly see that both these porous polymers have a high nitrogen content in the network. The nitrogen content of **TBAL-POP-2** is slightly greater than **TBAL-POP-1**. A calculated and measured CHN analysis of the two polymers and the corresponding monomer units is tabulated in Table S1 (Supplementary Note 6, ESI). We have been seen that the calculated and experimental data greatly matched with each other for monomer units. This analysis displays the excellent purity of the monomer unit before using the polymer network synthesis. The discrepancy between calculated and measured CHN analysis for both polymers will be attributed to the entrapment of the guest solvent or air molecules inside the porous network.[38,39] The thermal stability of the polymeric network is an essential feature for industrially relevant adsorbent materials. Thermogravimetric analysis (TGA)-differential thermal analysis plot (Figure 2d) shows that **TBAL-POP-1** and **2** polymers are stable up to 300 and 247 °C, respectively which suggests the good thermal stability of those POPs. Before reaching those temperatures, the continuous weight loss (1.31 and 5.96% for **TBAL-POP-1** and **2**, respectively) indicates the removal of water/guest solvent molecule from the porous architecture as it is not easy to remove the molecules from pores at moderate temperature, which is also explained before, during the CHN analysis.[38,39] For investigating the chemical stability, we have recorded the FT-IR spectra of those materials after soaking in 3 M HCl and NaOH solution for 1 day and treating with open air and boiling water for 7 days. From Figure S5 in ESI (Supplementary Note 7), we have seen that there is no change in the bonding connectivity throughout the framework. From this analysis, we can say that our materials are chemically stable.

Surface Area and Porosity Analysis. The porosity and surface area of these two porous polymers were investigated from the N_2 adsorption/desorption isotherms of **TBAL-POP-1** and **TBAL-POP-2** at 77 K (Figure 3a,c). These isotherms

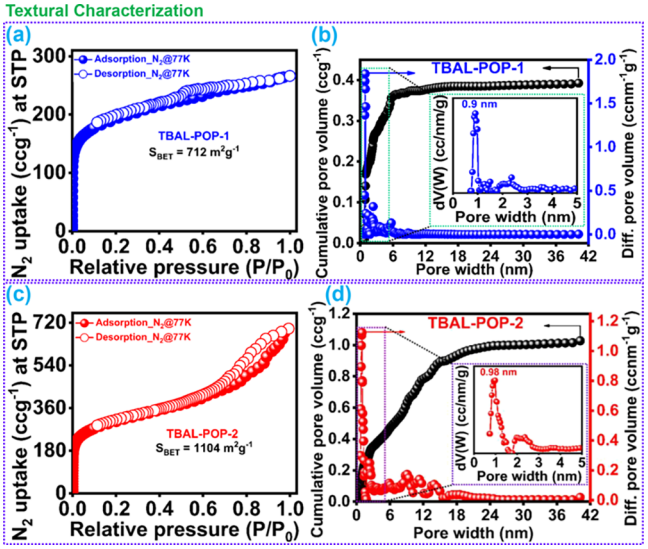

Figure 3. (a,c) N_2 adsorption/desorption isotherms of **TBAL-POP-1** and **TBAL-POP-2**, respectively; (b,d) pore size distribution and cumulative pore volume by the NLDFT method.

suggested that both the polymers show very steep uptake of N_2 gas at a very low relative pressure region ($P/P_0 < 0.01$) according to IUPAC classification,[40] indicating the presence of a large amount of micropores in the polymeric network. However, a significant hysteresis occurs in the case of **TBAL-POP-2**, suggesting that an elastic deformation or pore swelling happens during gas sorption.[41] The Brunauer−Emmett−Teller (BET) surface areas are 712 and 1104 m^2g^{-1} for **TBAL-POP-1** and **TBAL-POP-2**, respectively (ESI, Supplementary Note 8, Figures S6 and S7) with total pore volumes 0.392 and 1.032 ccg^{-1}.

The decrease in the BET surface area and pore volume in the case of **TBAL-POP-1** may be due to the contraction of the polymeric network as the network is formed by the linkage of hexamine (TPDATPA) with a small aldehyde group (HCHO). The pore size distributions of the porous polymers were calculated by using nonlocal density functional theory (NLDFT), and they showed major peaks centered at 0.9 and 0.98 nm for **TBAL-POP-1** and **TBAL-POP-2**, respectively (Figure 3b,d). **TBAL-POP-1** displayed the highest fraction of

https://doi.org/10.1021/acsami.3c11732
ACS Appl. Mater. Interfaces 2023, 15, 48326−48335

Table 1. Textural Properties of Two Triazine-Based Aminal Linkage POPs

samples	S_{BET} [$m^2\ g^{-1}$][a]	$S_{Langmuir}$ [$m^2\ g^{-1}$]	S_{micro} [$m^2\ g^{-1}$][b]	V_{micro} [ccg^{-1}][c]	V_{total} [ccg^{-1}][d]	pore width [nm]	S_{micrc}/S_{BET} [%]	V_{micro}/V_{total} [%]
TBAL-POP-1	712	849	488	0.204	0.392	0.90	68.5	51.9
TBAL-POP-2	1104	1376	587	0.249	1.032	0.98	53.2	24.2

[a]BET surface area. [b]Micropore surface area. [c]Micropore volume. [d]Total pore volume. [Note: micropore surface area and micropore volume were calculated by using the *t*-plot method (ESI, Supplementary Note 9, Figures S8 and S9).]

micropores (micropore volume of 0.204 ccg^{-1} occupying 51.9%) than **TBAL-POP-2** (micropore volume of 0.249 ccg^{-1} occupying 24.2%). Interparticle void space could be responsible for the presence of considerable mesopores[42] in **TBAL-POP-2**. Overall textural properties of the polymers are summarized in Table 1.

Electron Microscopic Analysis. The morphological and nanostructural features of **TBAL-POP-1** and **TBAL-POP-2** were investigated by using field emission scanning electron microscopy (FE-SEM) and high-resolution transmission electron microscopy (HR-TEM) techniques. FE-SEM images of the representative porous polymers are shown in Figure 4a,b.

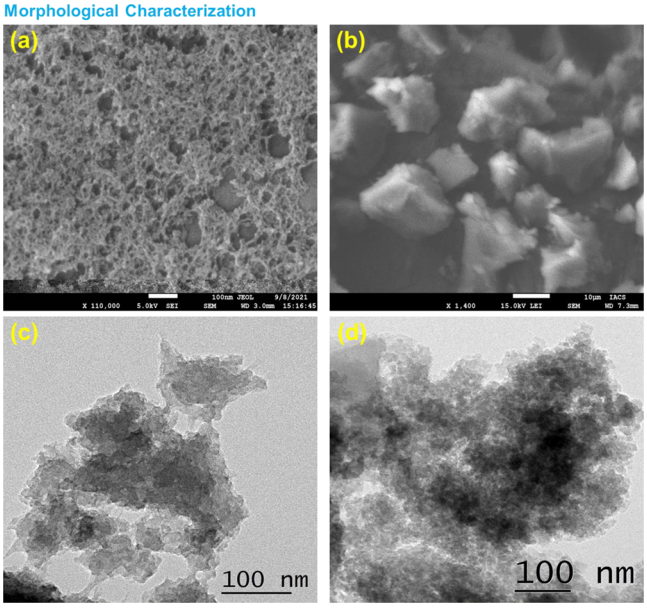

Figure 4. FE-SEM micrographs of **TBAL-POP-1** (a) and **TBAL-POP-2** (b); HR-TEM images of **TBAL-POP-1** (c) and **TBAL-POP-2** (d).

From the FE-SEM images, it was revealed that **TBAL-POP-1** has a spider-net-like morphology, whereas **TBAL-POP-2** exhibits a three-dimensional irregular morphology. The HR-TEM images of **TBAL-POP-1** and **2** are shown in Figure 4c,d, respectively, and they represent the thin sheetlike structures.

XPS Data Analysis. To establish the polymeric structure as well as constituting elements of the two TBAL-POPs, X-ray photoelectron spectroscopy (XPS) has been recorded. The full-range XPS spectra of **TBAL-POP-1** and **2** are shown in Figures S10a,b (Supplementary Note 10 in ESI), respectively. These spectra suggest the existence of C 1s, N 1s, and O 1s bands.[43−45]

When we deconvoluted the C 1s spectra (Figure 5a,c) of both polymers, the peaks were present at 284.19, 284.33, 286.06 and 284.11, 284.77, 286.09 eV for **TBAL-POP-1** and **2**, respectively, and these three peaks for each POP attribute corresponding to the binding energy of C═C (sp^2 C) bond of benzene, C═N bond, and C−CH−NH (sp^3 C) bond of the methylene moiety present in the polymeric network. Deconvolution of N 1s

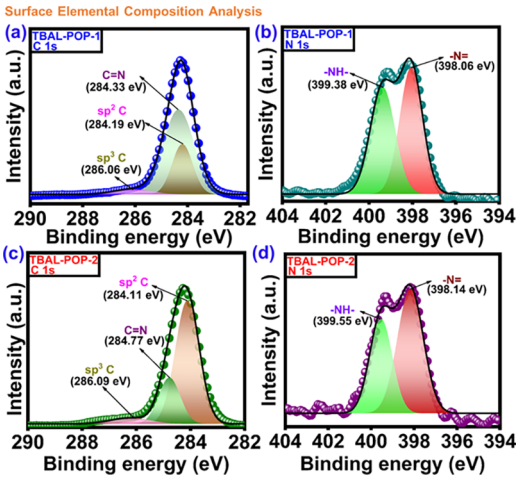

Figure 5. XPS high-resolution spectra of C 1s (a) and N 1s (b) of **TBAL-POP-1**; XPS high-resolution spectra of C 1s (c) and N 1s (d) spectra of **TBAL-POP-2**.

spectra of those polymers (Figure 5b,d) gives two separate bands located at 398.0−398.2 and 399.3−399.6 eV. The lower band (398.0−398.2 eV) reveals the existence of −N═ bond of the triazine moiety in the nanoporous framework of **TBAL-POP-1** and **TBAL-POP-2**. This peak also represents the −N═ bond of both triazines along with the tetrazole moiety. Another higher (399.6 eV) band could be attributed to the binding energy of the −NH− bond of the imine repeating unit of both polymeric networks.[43] The strong peak arises at the full range spectra of both polymers in Figure S10a,b (Supplementary Note 10 in ESI) at 530−532 eV for O 1s binding energy. This peak represents the oxygen peak of H_2O,[44] which comes from the pore-entrapped water molecule, and it is not easy to remove them from the voids of this porous organic polymer. This is also explained from the TGA and CHN analysis.[38,39] Thus, this XPS analysis confirms the formation of the polymeric structure very nicely.

High-Pressure Gas Uptake Analysis. Pure component CO_2 adsorption isotherms of the POPs **TBAL-POP-1** and **TBAL-POP-2** were investigated at 0, 25, and 40 °C within the pressure range 0−30 bar. The main focus is to investigate the CO_2 uptake at moderate-to-high pressure (10−30 bar) to mimic the precombustion CO_2 capture. The CO_2 uptake data of **TBAL-POP-1** (Figure 6a) shows that at 0 °C, a sharp uptake occurs and it captures 16.1 mmol g^{-1} (70.5 wt %) CO_2 at 30 bar pressure. Further, from the isotherm, it is clearly shown than the CO_2 uptake of the material did not reach the saturation level, suggesting that the materials also capture some more amount of CO_2 with increasing pressure. With increasing temperature, the CO_2 uptake capacity will decrease for **TBAL-POP-1**, i.e., 9.2 mmol g^{-1} at 25 °C/30 bar and 7.3 mmol g^{-1} at 40 °C/30 bar. The CO_2 uptake data of **TBAL-POP-2** are shown in Figure 6b. At 0, 25, and 40 °C temperatures and 30 bar pressure, CO_2 uptakes are 57.2, 18.7, and 15.9 mmol g^{-1}, respectively. We also

https://doi.org/10.1021/acsami.3c11732
ACS Appl. Mater. Interfaces 2023, 15, 48326−48335

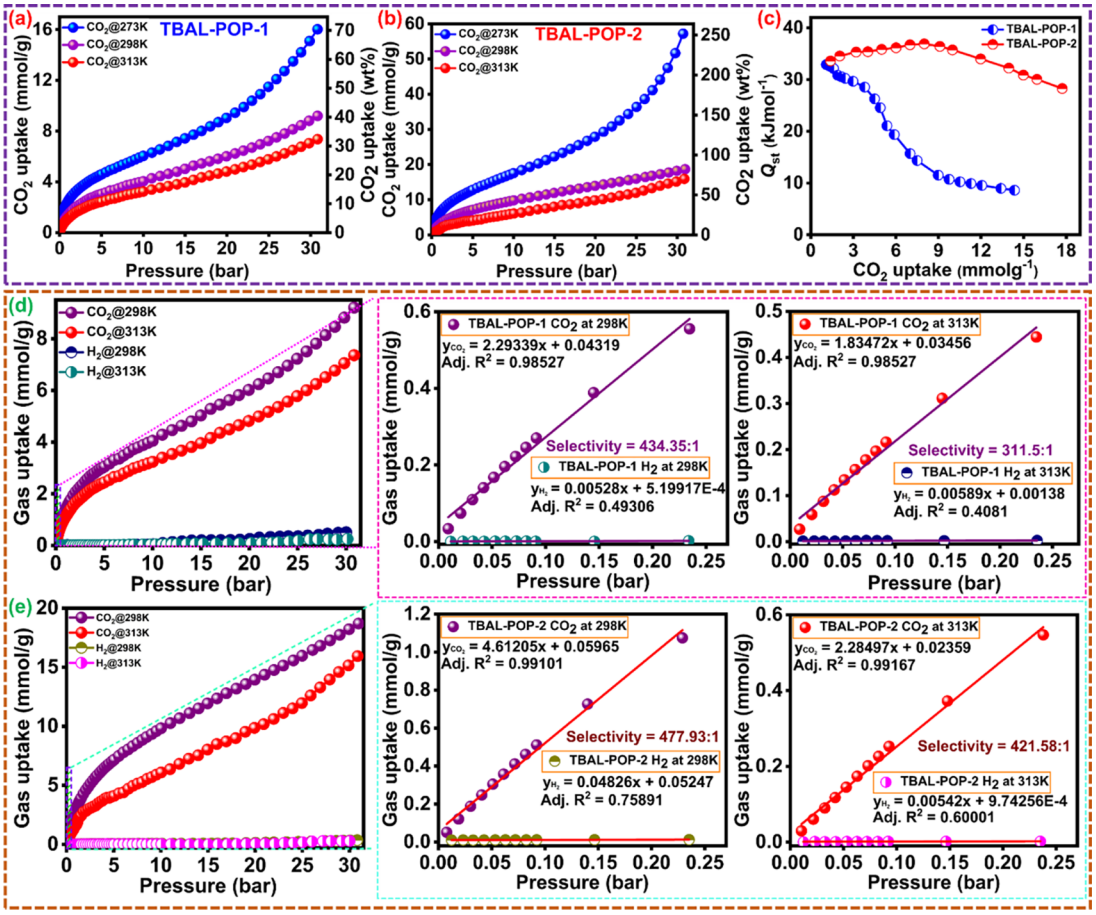

Figure 6. Demonstration of high-pressure CO_2 and H_2 uptake properties of two POPs: (a) CO_2 uptake data of **TBAL-POP-1** up to 30 bar pressure at different temperatures; (b) CO_2 uptake data of **TBAL-POP-2** up to 30 bar pressure at different temperatures; (c) heat of adsorption (Q_{st}) of **TBAL-POP-1** and **TBAL-POP-2;** (d) CO_2 and H_2 uptake data of **TBAL-POP-1** at 298 and 313 K (initial slope selectivity shown on the right side with an enlarged low-pressure region); (e) CO_2 and H_2 uptake data of **TBAL-POP-2** at 298 and 313 K (initial slope selectivity shown on the right side with an enlarged low-pressure region).

Table 2. CO_2 Uptake Capacity at Different Temperature and Pressures by Various Nanoporous Materials[a]

			CO_2 uptake (mmol g^{-1}) @1 bar				CO_2 uptake (mmol g^{-1}) high pressure				
entry	materials	S_{BET} (m^2g^{-1})	273 K	298 K	313 K	pressure (bar)	273 K	298 K	313 K	Q_{st} (kJ mol^{-1}) for CO_2 uptake	ref
1.	NDAB3- 500	1863	3.6	2.1		30	18.2	13.1		32.2	33
2.	MOF-177	4690				40			33.8		16
3.	rht-type MOF 1	3160	9.9	5.4		20	27.5	23.5		26.3	48
4.	ACGR4700	3144		4.1		20		20			49
5.	G-3.6-2	3460		1.5		50		49.1			50
6.	HCP-1	1646		1.7		30		13.3		23.5	19
7.	HNUST-7	2804	5.42			30	26.1	19.4		24.8	51
8.	SEW-MCN-1-130	655				30	15.4	6.4		34.44	52
9.	LSB3−800	2230	6.8	3.1		30	26.4	17.5		30.4	53
10.	**TBAL-POP-1**	**712**	**2.6**	**1.4**	**1.1**	**30**	**16.1**	**9.2**	**7.3**	**32.9**	**TW**
11.	**TBAL-POP-2**	**1104**	**5.0**	**3.9**	**1.9**	**30**	**57.2**	**18.7**	**15.9**	**33.7**	**TW**

[a]TW: this work.

need to find the CO_2-sorbent interaction ability of both polymers, which is predicted from the isosteric heat of adsorption (Q_{st}) value. The isosteric heat of adsorption was calculated from the Clausius−Clapeyron equation.[46] The Q_{st} vs CO_2 loading is demonstrated in Figure 6c, from which we see that the Q_{st} value of **TBAL-POP-1** is 32.9 kJ/mol. On the other hand, the **TBAL-POP-2** has a Q_{st} value of 33.7 kJ/mol at low CO_2 loading, and it is higher than that of **TBAL-POP-1** due to the presence of a large nitrogen (Lewis base) content in the porous network. From the Q_{st} values, we can conclude that the CO_2 adsorption by the polymers are purely physisorption and not chemisorption.[47] A detailed comparison is tabulated with the previously reported adsorbents for precombustion CO_2 capture in Table 2.

The selectivities of CO_2 over H_2 are calculated for both the polymers by the initial slope selectivity method from the pure

https://doi.org/10.1021/acsami.3c11732
ACS Appl. Mater. Interfaces 2023, 15, 48326−48335

Table 3. H_2 Uptake, CO_2/H_2 Selectivity, and Working Capacity in the CO_2 Capture for the Two POPs

samples	H_2 uptake (mmol g^{-1}) @30 bar		CO_2/H_2 selectivity (initial slope method)		working capacity (mmol/g) for 10 to 1 bar		working capacity (mmol/g) for 30 to 1 bar	
	298 K	313 K	298 K	313 K	298 K	313 K	298 K	313 K
TBAL-POP-1	0.51	0.25	434.35	296.92	2.73	2.11	7.79	6.23
TBAL-POP-2	0.36	0.29	477.93	421.58	6.73	4.42	15.61	14.23

CO_2 and H_2 adsorption isotherms (Figure 6d,e). The CO_2/H_2 selectivity of **TBAL-POP-1** is 434.35 and 311.5 at 298 and 313 K temperatures. On the other hand, the CO_2/H_2 selectivity of **TBAL-POP-2** is 477.93 and 421.58 at 298 and 313 K (Table 3). From the CO_2/H_2 selectivity value, we can conclude that the **TBAL-POP-2** is used as a better sorbent because the CO_2/H_2 selectivity value is the main parameter to judge a good sorbent. One of the important metric is the working capacity to select the potential sorbent materials capable for PSA. The working capacity in the PSA process is defined as the amount of CO_2 recovered in one adsorption desorption cycle. The working capacities of the above-mentioned porous polymers with pressure swings of 10 to 1 bar and 30 to 1 bar at 298 and 313 K temperatures are tabulated in Table 3. It is important to mention that **TBAL-POP-2** shows a good working capacity of 15.61 and 6.73 mmol/g for pressure swing 10 to 1 bar and 30 to 1 bar respectively, at 298 K temperature.

Here, we see that **TBAL-POP-2** shows the highest working capacity compared to **TBAL-POP-1** (Figure 7a,b). We have also

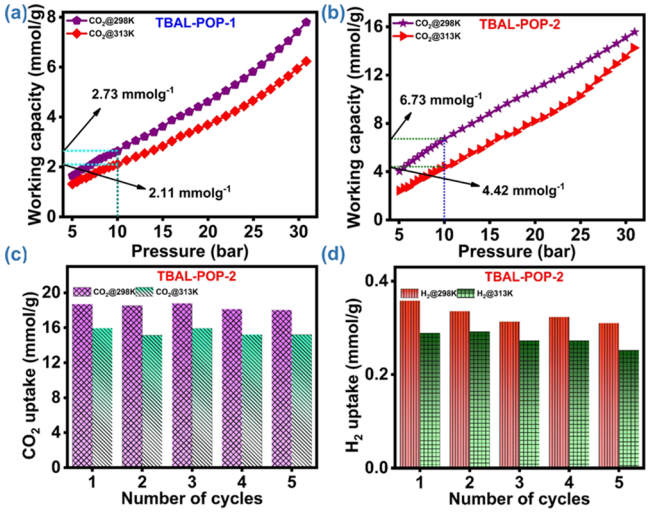

Figure 7. Certification for good sorbent materials in PSA: working capacity of **TBAL-POP-1** (a) and **TBAL-POP-2** (b). Recycling efficiency of CO_2 (c) and H_2 (d) uptakes at 298 and 313 K over TBAL-POP-2.

compared the working capacity of our materials with recently reported materials for H_2 purification by the PSA process, and our materials show excellent activity compared the others (Table S2, Supplementary Note 11, ESI).

Recycling Gas Uptake Analysis. All experimental data suggest that both the porous polymers (**TBAL-POP-1** and **TBAL-POP-2**) have significant CO_2 uptake capacity at high pressure. Further, the CO_2 and H_2 uptakes over **TBAL-POP-2** (Figure 7c,d) up to five consecutive cycles did not show any significant change. The recycling experiment was performed by degassing **TBAL-POP-2** material at 403 K for 4 h before each gas uptake cycle.

Ab Initio Quantum Chemical Calculation. Different configurations of 1:1, 1:2, 1:3, and 1:4 complexes between **TBAL-POP-1** or **TBAL-POP-2** model system and adsorbent (CO_2 or H_2) were optimized at the B3LYP/6-31+G(D,P) level of theory using the Gaussian quantum chemistry package.[54] Further, the bonding nature of various interactions between the adsorbed molecule (CO_2/H_2) and the model system was characterized using topological analyses of electron density by atoms in molecules (AIM) software.[54−61] The detailed methodology of such quantum chemical optimization and AIM analyses are described in Supplementary Note 12, ESI. The zero-point vibrational energy corrected stabilization energy of such complexes, along with the topological parameters estimated from the AIM analyses, are presented in Table S3 of Supplementary Note 12.

The topology of the electron density map corresponding to the least energy (most stable) CO_2 and H_2 adsorbed complexes of **TBAL-POP-1** and **TBAL-POP-2** is shown in Figure 8a, whereas all conformations for different size clusters are presented in the Supporting Information (Supplementary Note 12, Figures S11 and S12). Further, topological parameters estimated at the bond critical point (BCP) from the AIM analyses of the optimized complexes confirm that **TBAL-POP-1** and **TBAL-POP-2** model systems adsorb CO_2 by N−H···O_{CO2}, C−H···O_{CO2}, N···C_{CO2}, and N···O_{CO2} type of interaction with varying π/σ bond character suggesting different anisotropy of electron density at the BCP for these interactions. The electron density [$\rho(r)$] and Laplacian of electron density [$L(r)$] values greater than 0.002 and 0.02 along with positive $H(r)$ and $R(r) > 1$ [$R(r) = \left|\frac{G(r)}{V(r)}\right|$, $G(r)$ = kinetic energy density, and $V(r)$ = potential energy density of the electron] values at the BCP for all these interactions suggest that these interactions are weak noncovalent type.[55,56,62−65] These weak noncovalent interactions were previously reported for various systems.[62,63,65−68] Among these interactions, N−H···O_{CO2} between the CO_2 molecule and the material is the strongest one with a bond energy of ∼2.5 kcal.mol^{-1} and an epsilon value close to zero, suggesting predominant σ-bond character (see Table S2 for details). On the other hand, the H_2 adsorption takes place by the materials exclusively by the N···H_{H2} type of interaction between **TBAL-POP-1**/**TBAL-POP-2** and H_2 molecules as can be visible from Figure 8b. The topological parameters $\rho(r)$ and $L(r)$ are on the borderline to be considered as noncovalent interaction, suggesting that the N···H_{H2} type of interaction is extremely weak in nature, which are 2−3 times less strong compared to that for CO_2 adsorption by the material.

The weighted average complexation energy [ΔE_{Comp}^{WAvg}] for CO_2 and H_2 adsorption by **TBAL-POP-1** and **TBAL-POP-2** model system is shown in Figure 9, which becomes increasingly negative with the successive addition of CO_2/H_2 molecules to the complex, showing efficient CO_2 and H_2 adsorption by the material. However, ΔE_{Comp}^{WAvg} for the CO_2 adsorption is about 3−5 times more negative compared to that for H_2 adsorption for the identical cluster size, indicating superior selectivity of CO_2

https://doi.org/10.1021/acsami.3c11732
ACS Appl. Mater. Interfaces 2023, 15, 48326−48335

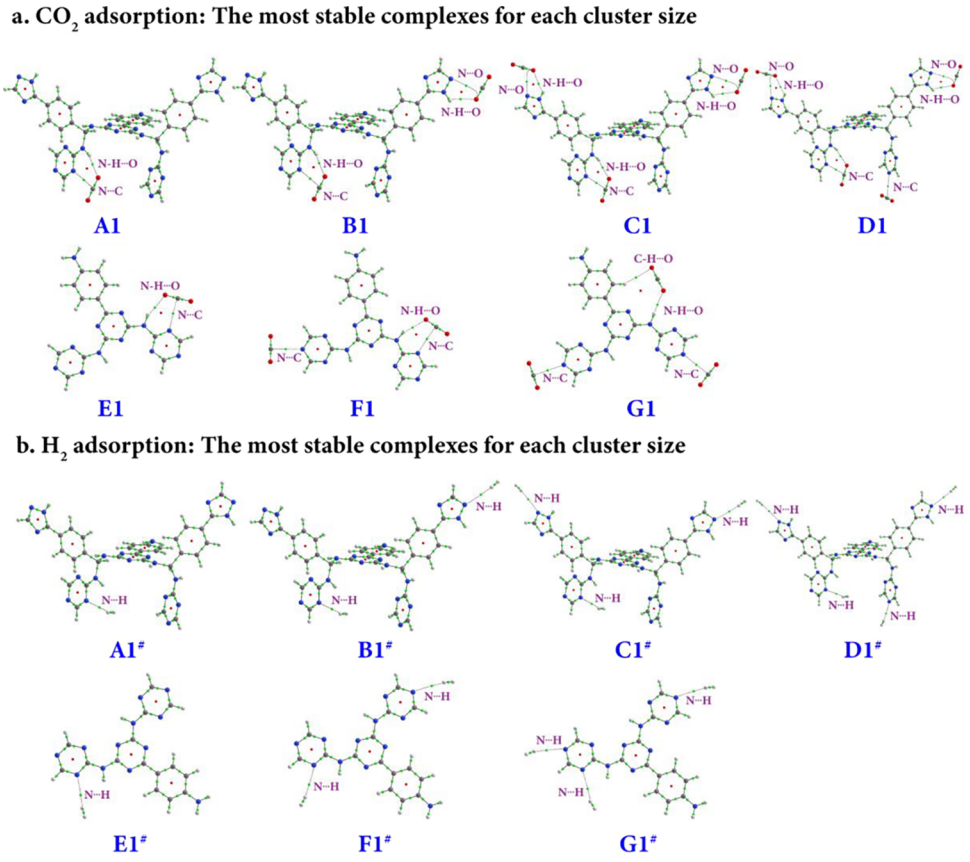

Figure 8. A1, B1, C1, and D1 in (a) represent the most stable (least energy) 1:1, 1:2, 1:3, and 1:4 complexes between **TBAL-POP-2** model system and CO_2, whereas A1$^{\#}$, B1$^{\#}$, C1$^{\#}$, and D1$^{\#}$ in (b) correspond to the most stable complexes between **TBAL-POP-2** model system and H_2. Similarly, E1, F1, and G1 in (a) represent the most stable 1:1, 1:2, and 1:3 complexes between **TBAL-POP-1** and CO_2, whereas E1$^{\#}$, F1$^{\#}$, and G1$^{\#}$ in (b) correspond to the most stable complexes between **TBAL-POP-1** and the H_2 molecule.

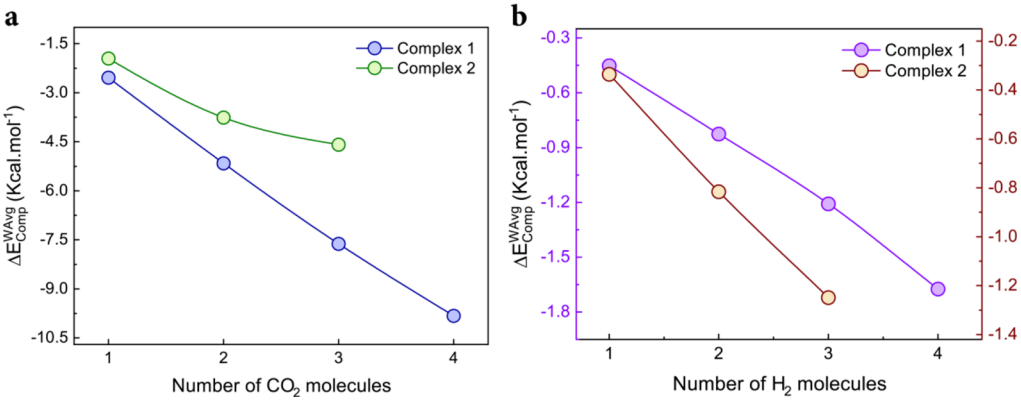

Figure 9. Weighted average complexation energy [ΔE_{Comp}^{WAvg}] for (a) CO_2 and (b) H_2 adsorption by **TBAL-POP-1** and **TBAL-POP-2** model systems.

adsorption by the material compared to the H_2 adsorption which is in good agreement with the experimental data as well as computed topological parameters at the BCP (see Tables S2 and S3 for details).

CONCLUSIONS

Hydrogen is a green fuel and sustainable source of energy. Hence, the purification of hydrogen from the CO_2/H_2 gas mixture that is produced in the steam reforming process is a great challenge. For this, a good solid sorbent material having high CO_2 capture efficiency is required. We found a nitrogen-rich porous organic polymer **TBAL-POP-2** synthesized through the condensation of a tetramine and 4-(1H-tetrazol-5-yl)-benzaldehyde as an excellent sorbent that effectively separates H_2 from the CO_2/H_2 gas mixture. Aminal-linked porous framework with a high nitrogen content, a large mesopore volume, and a high BET surface area of **TBAL-POP-2** could be responsible for its high CO_2/H_2 selectivity of 477.93 (298 K) and 421.58 (313 K) as well as the high working capacity (15.61 mmol g^{-1} at 298 K for 30 bar to 1 bar pressure swing). High CO_2 capture efficiency of this aminal-linked porous organic polymer with an excellent CO_2/H_2 separation efficiency could offer an ideal solution for the industrially relevant precombustion CO_2 capture and hydrogen purification process in the future.

https://doi.org/10.1021/acsami.3c11732
ACS Appl. Mater. Interfaces 2023, 15, 48326−48335

■ ASSOCIATED CONTENT

Supporting Information

The Supporting Information is available free of charge at https://pubs.acs.org/doi/10.1021/acsami.3c11732.

General information, materials synthesis, ^{1}H NMR spectra, PXRD, surface area calculation from N_2-sorption isotherms, comparison of working capacity with high performing sorbent materials for H_2 purification, ab initio quantum chemical calculations, and AIM analyses (PDF)

■ AUTHOR INFORMATION

Corresponding Author

Asim Bhaumik − *School of Materials Sciences, Indian Association for the Cultivation of Science, Kolkata 700032, India;* orcid.org/0000-0002-4907-7418; Email: msab@iacs.res.in

Authors

Debabrata Chakraborty − *School of Materials Sciences, Indian Association for the Cultivation of Science, Kolkata 700032, India*

Rupak Chatterjee − *School of Materials Sciences, Indian Association for the Cultivation of Science, Kolkata 700032, India;* orcid.org/0000-0002-3325-7895

Saptarsi Mondal − *Center for Molecular Spectroscopy and Dynamics, Institute of Basic Science (IBS), Seoul 02841, Republic of Korea; Department of Chemistry, Korea University, Seoul 02841, Republic of Korea;* orcid.org/0000-0003-1140-9322

Sabuj Kanti Das − *School of Materials Sciences, Indian Association for the Cultivation of Science, Kolkata 700032, India;* orcid.org/0000-0003-1284-385X

Vipin Amoli − *Department of Sciences & Humanities, Rajiv Gandhi Institute of Petroleum Technology, Amethi, Uttar Pradesh 229304, India*

Minhaeng Cho − *Center for Molecular Spectroscopy and Dynamics, Institute of Basic Science (IBS), Seoul 02841, Republic of Korea; Department of Chemistry, Korea University, Seoul 02841, Republic of Korea;* orcid.org/0000-0003-1618-1056

Complete contact information is available at: https://pubs.acs.org/10.1021/acsami.3c11732

Author Contributions

$^{\perp}$D.C. and R.C. contributed equally to this paper.

Notes

The authors declare no competing financial interest.

■ ACKNOWLEDGMENTS

D.C. and R.C. would like to acknowledge the DST-INSPIRE and CSIR, New Delhi, respectively, for their Senior Research Fellowships. A.B. thanks the DST, New Delhi, for the DST-SERB core research grant (project no. CRG/2022/002812). V.A. wants to express his gratitude to the Central Instrumentation Facilities at the Rajiv Gandhi Institute of Petroleum Technology, Uttar Pradesh, India.

■ REFERENCES

(1) https://www.co2.earth/daily-co2 (accessed Feb 11, 2023), DOI: 10.1016/j.canep.2023.102452.

(2) Bernstein, L.; Bosch, P.; Canziani, O.; Chen, Z.; Christ, R.; Riahi, K. *IPCC, 2007: Climate Change 2007: Synthesis Report*; IPCC, 2008, DOI: 10.1038/onc.2009.348.

(3) Legg, S. IPCC, 2021: Climate Change 2021-the Physical Science basis. *Interaction* **2021**, *49*, 44−45.

(4) Metz, B.; Davidson, O.; De Coninck, H.; Loos, M.; Meyer, L. *IPCC, 2005: IPCC Special Report on Carbon Dioxide Capture and Storage; Prepared by Working Group III of the Intergovernmental Panel on Climate Change*; Cambridge University Press: Cambridge, United Kingdom and New York, NY, USA, 2005.

(5) Coromina, H. M.; Walsh, D. A.; Mokaya, R. Biomass-Derived Activated Carbon with Simultaneously Enhanced CO_2 Uptake for Both Pre and Post Combustion Capture Applications. *J. Mater. Chem. A* **2016**, *4*, 280−289.

(6) Schell, J.; Casas, N.; Pini, R.; Mazzotti, M. Pure and Binary Adsorption of CO_2, H_2, and N_2 on Activated Carbon. *Adsorption* **2012**, *18*, 49−65.

(7) Herm, Z. R.; Krishna, R.; Long, J. R. CO_2/CH_4, CH_4/H_2 and $CO_2/CH_4/H_2$ Separations at High Pressures Using Mg_2(Dobdc). *Microporous Mesoporous Mater.* **2012**, *151*, 481−487.

(8) Wang, Y. T.; McHale, C.; Wang, X.; Chang, C. K.; Chuang, Y. C.; Kaveevivitchai, W.; Miljanić, O.; Chen, T. H. Cyclotetrabenzoin Acetate: A Macrocyclic Porous Molecular Crystal for CO_2 Separations by Pressure Swing Adsorption. *Angew. Chem., Int. Ed.* **2021**, *60*, 14931−14937.

(9) Sekizkardes, A. K.; Islamoğlu, T.; Kahveci, Z.; El-Kaderi, H. M. Application of Pyrene-Derived Benzimidazole-Linked Polymers to CO_2 Separation under Pressure and Vacuum Swing Adsorption Settings. *J. Mater. Chem. A* **2014**, *2*, 12492−12500.

(10) Kim, C.; Cho, H. S.; Chang, S.; Cho, S. J.; Choi, M. An Ethylenediamine-Grafted Y Zeolite: A Highly Regenerable Carbon Dioxide Adsorbent: via Temperature Swing Adsorption without Urea Formation. *Energy Environ. Sci.* **2016**, *9*, 1803−1811.

(11) Choi, W.; Min, K.; Kim, C.; Ko, Y. S.; Jeon, J. W.; Seo, H.; Park, Y. K.; Choi, M. Epoxide-Functionalization of Polyethyleneimine for Synthesis of Stable Carbon Dioxide Adsorbent in Temperature Swing Adsorption. *Nat. Commun.* **2016**, *7*, 12640 DOI: 10.1038/ncomms12640.

(12) García, S.; Pis, J. J.; Rubiera, F.; Pevida, C. Predicting Mixed-Gas Adsorption Equilibria on Activated Carbon for Precombustion CO_2 Capture. *Langmuir* **2013**, *29*, 6042−6052.

(13) Sumida, K.; Rogow, D. L.; Mason, J. A.; McDonald, T. M.; Bloch, E. D.; Herm, Z. R.; Bae, T. H.; Long, J. R. Carbon Dioxide Capture in Metal-Organic Frameworks. *Chem. Rev.* **2012**, *112*, 724−781.

(14) Akten, E. D.; Siriwardane, R.; Sholl, D. S. Monte Carlo Simulation of Single- and Binary-Component Adsorption of CO_2, N_2, and H_2 in Zeolite Na-4A. *Energy Fuels* **2003**, *17*, 977−983.

(15) Cao, D.; Wu, J. Modeling the Selectivity of Activated Carbons for Efficient Separation of Hydrogen and Carbon Dioxide. *Carbon* **2005**, *43*, 1364−1370.

(16) Herm, Z. R.; Swisher, J. A.; Smit, B.; Krishna, R.; Long, J. R. Metal-Organic Frameworks as Adsorbents for Hydrogen Purification and Precombustion Carbon Dioxide Capture. *J. Am. Chem. Soc.* **2011**, *133*, 5664−5667.

(17) Nandi, S.; De Luna, P.; Daff, T. D.; Rother, J.; Liu, M.; Buchanan, W.; Hawari, A. I.; Woo, T. K.; Vaidhyanathan, R. A Single-Ligand Ultra-Microporous MOF for Precombustion CO_2 Capture and Hydrogen Purification. *Sci. Adv.* **2015**, *1*, No. 1500421, DOI: 10.1126/sciadv.1500421.

(18) Deria, P.; Mondloch, J. E.; Tylianakis, E.; Ghosh, P.; Bury, W.; Snurr, R. Q.; Hupp, J. T.; Farha, O. K. Perfluoroalkane Functionalization of NU-1000 via Solvent-Assisted Ligand Incorporation: Synthesis and CO_2 Adsorption Studies. *J. Am. Chem. Soc.* **2013**, *135*, 16801−16804.

(19) Martín, C. F.; Stöckel, E.; Clowes, R.; Adams, D. J.; Cooper, A. I.; Pis, J. J.; Rubiera, F.; Pevida, C. Hypercrosslinked Organic Polymer Networks as Potential Adsorbents for Pre-Combustion CO_2 Capture. *J. Mater. Chem.* **2011**, *21*, 5475−5483.

(20) Jiang, J.-X.; Su, F.; Trewin, A.; Wood, C. D.; Campbell, N. L.; Niu, H.; Dickinson, C.; Ganin, A. Y.; Rosseinsky, M. J.; Khimyak, Y. Z.; Cooper, A. I. Conjugated Microporous Poly(Aryleneethynylene) Networks. *Angew. Chem., Int. Ed.* **2007**, *119*, 8728−8732, DOI: 10.1002/ange.200701595.
(21) Modak, A.; Nandi, M.; Mondal, J.; Bhaumik, A. Porphyrin Based Porous Organic Polymers: Novel Synthetic Strategy and Exceptionally High CO_2 Adsorption Capacity. *Chem. Commun.* **2012**, *48*, 248−250.
(22) Suresh, V. M.; Bonakala, S.; Atreya, H. S.; Balasubramanian, S.; Maji, T. K. Amide Functionalized Microporous Organic Polymer (Am-MOP) for Selective CO_2 Sorption and Catalysis. *ACS Appl. Mater. Interfaces* **2014**, *6*, 4630−4637.
(23) Das, S. K.; Bhanja, P.; Kundu, S. K.; Mondal, S.; Bhaumik, A. Role of Surface Phenolic-OH Groups in N-Rich Porous Organic Polymers for Enhancing the CO_2 Uptake and CO_2/N_2 Selectivity: Experimental and Computational Studies. *ACS Appl. Mater. Interfaces* **2018**, *10*, 23813−23824.
(24) Qi, S. C.; Wu, J. K.; Lu, J.; Yu, G. X.; Zhu, R. R.; Liu, Y.; Liu, X. Q.; Sun, L. B. Underlying Mechanism of CO_2 Adsorption onto Conjugated Azacyclo-Copolymers: N-Doped Adsorbents Capture CO_2 Chiefly through Acid−Base Interaction. *J. Mater. Chem. A* **2019**, *7*, 17842−17853.
(25) Jung, D.; Chen, Z. J.; Alayoglu, S.; Mian, M. R.; Goetjen, T. A.; Idrees, K. B.; Kirlikovali, K. O.; Islamoglu, T.; Farha, O. K. Postsynthetically Modified Polymers of Intrinsic Microporosity (PIMs) for Capturing Toxic Gases. *ACS Appl. Mater. Interfaces* **2021**, *13*, 10409−10415.
(26) Chowdhury, A.; Bhattacharjee, S.; Chatterjee, R.; Bhaumik, A. A New Nitrogen Rich Porous Organic Polymer for Ultra-High CO_2 Uptake and as an Excellent Organocatalyst for CO_2 Fixation Reactions. *J. CO2 Util.* **2022**, *65*, No. 102236.
(27) Qi, S. C.; Yu, G. X.; Xue, D. M.; Liu, X.; Liu, X. Q.; Sun, L. B. Rigid Supramolecular Structures Based on Flexible Covalent Bonds: A Fabrication Mechanism of Porous Organic Polymers and Their CO_2 Capture Properties. *Chem. Eng. J.* **2020**, *385*, No. 123978.
(28) Lyu, H.; Li, H.; Hanikel, N.; Wang, K.; Yaghi, O. M. Covalent Organic Frameworks for Carbon Dioxide Capture from Air. *J. Am. Chem. Soc.* **2022**, *144*, 12989−12995.
(29) Yang, L.; Yang, H.; Wu, H.; Zhang, L.; Ma, H.; Liu, Y.; Wu, Y.; Ren, Y.; Wu, X.; Jiang, Z. COF Membranes with Uniform and Exchangeable Facilitated Transport Carriers for Efficient Carbon Capture. *J. Mater. Chem. A* **2021**, *9*, 12636−12643.
(30) Yang, S. A.; Zhu, W. C.; Zhu, L. B.; Ma, X.; Yan, T. A.; Gu, N. C.; Lan, Y. S.; Huang, Y.; Yuan, M. Y.; Tong, M. M. Multi-Scale Computer-Aided Design of Covalent Organic Frameworks for CO_2 Capture in Wet Flue Gas. *ACS Appl. Mater. Interfaces* **2022**, *14*, 56353−56362.
(31) EL-Mahdy, A. F. M.; Kuo, C.-H.; Alshehri, A.; Young, C.; Yamauchi, Y.; Kim, J.; Kuo, S.-W. Strategic Design of Triphenylamine- and Triphenyltriazine-Based Two-Dimensional Covalent Organic Frameworks for CO_2 Uptake and Energy Storage. *J. Mater. Chem. A* **2018**, *6*, 19532−19541.
(32) Nandi, S.; Rother, J.; Chakraborty, D.; Maity, R.; Zwanziger, U. W.; Vaidhyanathan, R. Exceptionally Stable Bakelite-type Polymers for Efficient Pre-Combustion CO_2 Capture and H_2 Purification. *J. Mater. Chem. A* **2017**, *5*, 8431−8439.
(33) Singh, G.; Kim, I. Y.; Lakhi, K. S.; Joseph, S.; Srivastava, P.; Naidu, R.; Vinu, A. Heteroatom Functionalized Activated Porous Biocarbons and their Excellent Performance for CO_2 Capture at High Pressure. *J. Mater. Chem. A* **2017**, *5*, 21196−21204.
(34) Sharma, S. K.; Khan, T. S.; Singha, R. K.; Paul, B.; Poddar, M. K.; Sasaki, T.; Bordoloi, A.; Samanta, C.; Gupta, S.; Bal, R. Design of Highly Stable MgO Promoted Cu/ZnO Catalyst for Clean Methanol Production through Selective Hydrogenation of CO_2. *Appl. Catal., A* **2021**, *623*, No. 118239.
(35) Sabri, M. A.; Al-Sayah, M. H.; Sen, S.; Ibrahim, T. H.; El-Kadri, O. M. Fluorescent Aminal Linked Porous Organic Polymer for Reversible Iodine Capture and Sensing. *Sci. Rep.* **2020**, *10*, 15943 DOI: 10.1038/s41598-020-72697-x.
(36) Abdelmoaty, Y. H.; Tessema, T. D.; Choudhury, F. A.; ElKadri, O. M.; El-Kaderi, H. M. Nitrogen-Rich Porous Polymers for Carbon Dioxide and Iodine Sequestration for Environmental Remediation. *ACS Appl. Mater. Interfaces* **2018**, *10*, 16049−16058.
(37) Mittal, R.; Awasthi, S. K. A Synergistic Magnetically Retrievable Inorganic-Organic Hybrid Metal Oxide Catalyst for Scalable Selective Oxidation of Alcohols to Aldehydes and Ketones. *ChemCatChem* **2021**, *13*, 4799−4813.
(38) Dawson, R.; Cooper, A. I.; Adams, D. J. Nanoporous Organic Polymer Networks. *Prog. Polym. Sci.* **2012**, *37*, 530−563.
(39) Yuan, S.; Dorney, B.; White, D.; Kirklin, S.; Zapol, P.; Yu, L.; Liu, D. J. Microporous Polyphenylenes with Tunable Pore Size for Hydrogen Storage. *Chem. Commun.* **2010**, *46* (25), 4547−4549.
(40) Sing, K. S. W.; Everett, D. H.; Haul, R. A. W.; Moscou, L.; Pierotti, R. A.; Rouquerol, J.; Siemieniewska, T. Reporting Physisorption Data For Gas/Solid Systems with Special Reference to the Determination of Surface Area and Porosity. *Pure Appl. Chem.* **1985**, *57*, 603−619.
(41) Weber, J.; Antonietti, M.; Thomas, A. Microporous Networks of High-Performance Polymers: Elastic Deformations and Gas Sorption Properties. *Macromolecules* **2008**, *41*, 2880−2885.
(42) Dutta, A.; Mondal, J.; Patra, A. K.; Bhaumik, A. Synthesis and Temperature-Induced Morphological Control in a Hybrid Porous Iron-Phosphonate Nanomaterial and Its Excellent Catalytic Activity in the Synthesis of Benzimidazoles. *Chem.—Eur. J.* **2012**, *18*, 13372−13378.
(43) Shao, L.; Liu, M.; Sang, Y.; Huang, J. One-pot Synthesis of Melamine-based Porous Polyamides for CO_2 Capture. *Microporous Mesoporous Mater.* **2019**, *285*, 105−111.
(44) Dinh, C.-T.; Jain, A.; de Arquer, F. P. G.; De Luna, P.; Li, J.; Wang, N.; Zheng, X.; Cai, J.; Gregory, B. Z.; Voznyy, O.; Zhang, B.; Liu, M.; Sinton, D.; Crumlin, E. J.; Sargent, E. H. Multi-site Electrocatalysts for Hydrogen Evolution in Neutral Media by Destabilization of Water Molecules. *Nat. Energy* **2019**, *4*, 107−114.
(45) Mousa, A. O.; Mohamed, M. G.; Chuang, C. H.; Kuo, S. W. Carbonized Aminal-Linked Porous Organic Polymers Containing Pyrene and Triazine Units for Gas Uptake and Energy Storage. *Polymers* **2023**, *15*, 1891.
(46) Shen, D.; Bulow, M.; Siperstein, F.; Engelhard, M.; Myers, A. L. Comparison of Experimental Techniques for Measuring Isosteric Heat of Adsorption. *Adsorption* 2000, *6*, 275−286, DOI: 10.1023/A:1026551213604
(47) Dawson, R.; Adams, D. J.; Cooper, A. I. Chemical Tuning of CO_2 Sorption in Robust Nanoporous Organic Polymers. *Chem. Sci.* **2011**, *2*, 1173−1177.
(48) Zheng, B.; Bai, J.; Duan, J.; Wojtas, L.; Zaworotko, M. J. Enhanced CO_2 Binding Affinity of a High-Uptake rht-Type Metal-Organic Framework Decorated with Acylamide Groups. *J. Am. Chem. Soc.* **2011**, *133*, 748−751.
(49) Coromina, H. M.; Walsh, D. A.; Mokaya, R. Biomass-Derived Activated Carbon with Simultaneously Enhanced CO_2 Uptake for Both Pre and Post Combustion Capture Applications. *J. Mater. Chem. A* **2016**, *4*, 280−289, DOI: 10.1039/C5TA09202G.
(50) Sevilla, M.; Al-Jumialy, A. S. M.; Fuertes, A. B.; Mokaya, R. Optimization of the Pore Structure of Biomass-Based Carbons in Relation to Their Use for CO_2 Capture under Low- and High-Pressure Regimes. *ACS Appl. Mater. Interfaces* **2018**, *10*, 1623−1633.
(51) Zheng, B.; Huang, L.; Cao, X.; Shen, S.; Cao, H.; Hang, C.; Zeng, W.; Wang, Z. A Highly Porous Acylamide Decorated MOF-505 Analogue Exhibiting Large and Selective CO_2 Gas Uptake Capability. *CrystEngComm* **2018**, *20*, 1874−1881.
(52) Lakhi, K. S.; Park, D.; Singh, G.; Talapaneni, S. N.; Ravon, U.; Al-Bahily, K.; Vinu, A. Energy efficient Synthesis of Highly Ordered Mesoporous Carbon Nitrides with Uniform Rods and their Superior CO_2 Adsorption Capacity. *J. Mater. Chem. A* **2017**, *5*, 16220−16230.
(53) Singh, G.; Lakhi, K. S.; Ramadass, K.; Sathish, C. I.; Vinu, A. High-Performance Biomass-Derived Activated Porous Biocarbons for Combined Pre- and Post-Combustion CO_2 Capture. *ACS Sustain. Chem. Eng.* **2019**, *7*, 7412−7420.

(54) Frisch, M. J.; Trucks, G. W.; Schlegel, H. B.; Scuseria, G. E.; Robb, M. A.; Cheeseman, J. R.; Scalmani, G.; Barone, V.; Petersson, G. A.; Nakatsuji, H.; Li, X.; Caricato, M.; Marenich, A.; Bloino, J.; Janesko, B. G.; Gomperts, R.; Mennucci, B.; Hratchian, H. P.; Ortiz, J. V.; Izmaylov, A. F.; Sonnenberg, J. L.; Williams-Young, D.; Ding, F.; Lipparini, F.; Egidi, F.; Goings, J.; Peng, B.; Petrone, A.; Henderson, T.; Ranasinghe, D.; Zakrzewski, V. G.; Gao, J.; Rega, N.; Zheng, G.; Liang, W.; Hada, M.; Ehara, M.; Toyota, K.; Fukuda, R.; Hasegawa, J.; Ishida, M.; Nakajima, T.; Honda, Y.; Kitao, O.; Nakai, H.; Vreven, T.; Throssell, K.; Montgomery, J. A., Jr.; Peralta, J. E.; Ogliaro, F.; Bearpark, M.; Heyd, J. J.; Brothers, E. N.; Kudin, K. N.; Staroverov, V. N.; Keith, T. A.; Kobayashi, R.; Normand, J.; Raghavachari, K.; Rendell, A. P.; Burant, J. C.; Iyengar, S. S.; Tomasi, J.; Cossi, M.; Millam, J. M.; Klene, M.; Adamo, C.; Cammi, R.; Ochterski, J. W.; Martin, R. L.; Morokuma, K.; Farkas, O.; Foresman, J. B.; Fox, D. J. *Gaussian 16, revision C.01*; Gaussian, Inc.: Wallingford, CT, 2016.
(55) Popelier, P. L. A. Characterization of a Dihydrogen Bond on the Basis of the Electron Density. *J. Phys. Chem. A* **1998**, *102*, 1873−1878.
(56) Koch, U.; Popelier, P. L. A. Characterization of C-H-O Hydrogen Bonds on the Basis of the Charge Density. *J. Phys. Chem.* **1995**, *99*, 9747−9754.
(57) Bader, R. F. W. The Density in Density Functional Theory. *Comp. Theor. Chem.* **2010**, *943*, 2−18.
(58) Bader, R. F. W. Bond Paths Are Not Chemical Bonds. *J. Phys. Chem. A* **2009**, *113*, 10391−10396.
(59) Matta, C. F.; Bader, R. F. W. An Experimentalist's Reply to "What Is an Atom in a Molecule? *J. Phys. Chem. A* **2006**, *110*, 6365−6371.
(60) Bader, R. F. W.; Fang, D.-C. J. Properties of Atoms in Molecules: Caged Atoms and the Ehrenfest Force. *Chem. Theory Comput.* **2005**, *1*, 403−414.
(61) Bader, R. F. W. A Quantum Theory of Molecular Structure and its Applications. *Chem. Rev.* **1991**, *91*, 893−928.
(62) Mondal, S.; Singh, P. C. Noble Gas Induced Surprisingly Higher Stability of π Hydrogen Bonded Complex: Comparative Study of Hydrogen Bonded Complexes of HKrCCH and HCCH with H_2O, NH_3, CH_3OH and CH_3NH_2. *RSC Adv.* **2014**, *4*, 20752−20760.
(63) Mondal, S. Charge-Shifted Weak Noncovalent Interactions in the Atmospherically Important OCS Microhydrates. *J. Phys. Chem. A* **2023**, *127*, 3293−3304.
(64) Mondal, S.; Biswas, B.; Nandy, T.; Singh, P. C. Understanding the Role of Hydrophobic Terminal in the Hydrogen Bond Network of the Aqueous Mixture of 2,2,2-Trifluoroethanol: IR, Molecular Dynamics, Quantum Chemical as Well as Atoms in Molecules Studies. *J. Phys. Chem. B* **2018**, *122*, 6616−6626.
(65) Mondal, S.; Teja, A. U.; Singh, P. C. Theoretical Study on the Microhydration of Atmospherically Important Carbonyl Sulfide in Its Neutral and Anionic Forms: Bridging the Gap between the Bulk and Finite Size Microhydrated Cluster. *J. Phys. Chem. A* **2015**, *119*, 3644−3652.
(66) Mondal, S.; Kang, J.; Park, K.; Lim, J. M.; Ha, J.-H.; Kwak, K.; Cho, M. Adsorbed Water Structure on Acrylate-Based Biocompatible Polymer Surface. *J. Phys. Chem. Lett.* **2021**, *12*, 9275−9282.
(67) Mondal, S.; Chatterjee, S.; Halder, R.; Jana, B.; Singh, P. C. Role of Dispersive Fluorous Interaction in the Solvation Dynamics of the Perfluoro Group Containing Molecules. *J. Phys. Chem. B* **2017**, *121*, 7681−7688.
(68) Mondal, S.; Biswas, B.; Nandy, T.; Singh, P. C. Hydrophobic Fluorine Mediated Switching of the Hydrogen Bonding Site as well as Orientation of Water Molecules In The Aqueous Mixture of Monofluoroethanol: IR, Molecular Dynamics and Quantum Chemical Studies. *Phys. Chem. Chem. Phys.* **2017**, *19*, 24667−24677.

https://doi.org/10.1021/acsami.3c11732
ACS Appl. Mater. Interfaces 2023, 15, 48326−48335